

Fluid Flow And Heat Transfer Analysis Of Turbulent Multiple Circular Jets Impinging On A Flat Plate

K. DURGA PRASAD

P.G. Student

Dept. of Mechanical Engg., V.R. Siddhartha Engineering College, Vijayawada

K. RAVI KUMAR

Assistant Professor

Dept. of Mechanical Engg., V.R. Siddhartha Engineering College, Vijayawada

M.R.CH. SASTRY

Associate Professor

Dept. of Mechanical Engg., Gudlavalleru Engineering College Gudlavalleru

Abstract

Computations and Experiment investigations on a Flat plate and reported with constant heat flux imposed on bottom surface and five circular jets impinges on a top surface .The five circular jets consists of a central jet surrounded by four neighboring perimeter jets .Lampblack flow visualization technique and computation using shear stress transformation ($K-\omega$) turbulent model and employed to describe the complex interaction of the wall jets and the associated flow structure.

It is observed that the flow topology is practical independent of Reynolds number with in the investigation range but is significantly attend with the spacing between jet orifice and target surface. Primary pressure peaks are observed at the stagnation point and the secondary peaks are noticed at the interaction points of wall jets. A strong correlation between nusselt number and the pressure distribution is noticed.

Keywords: Jet impingement, array jet, flow visualization, Experiments, CFD

1. Introduction

Jet impingement flows are frequently used in various industrial equipment for their superior heat and mass transfer characteristics compared to those obtained for the same amount of gas flowing parallel to the target surface. Impinging jets are used in a wide variety of applications such as cooling of electronics and turbine blades, and in the heating, cooling, or drying of pulp, paper and textile. The ability to control heat transfer from the surface by varying flow parameters such as jet exit velocity and geometrical parameters such as jet exit opening, jet-to-plate spacing, and nozzle-to-nozzle spacing in arrays are some of the key factors that have lead to the sustained and widespread use of jet impingement

technologies. Jet impingement is used as an effective mechanism for achieving high localized transport rates. Single and multiple rows of jets are used to achieve this objective. The most commonly used geometries are axisymmetric (circular orifice or pipe), slot (two-dimensional) nozzles, rectangular (three-dimensional) and square (three-dimensional) nozzles.

The broad objectives of the paper are therefore to computationally investigate (i) the flow structure of the interacting jets experimentally by oil lampblack technique, and computation. (ii) The effect of varying h/d and Reynolds number on pressure distribution and heat transfer. Flow visualization experiments with oil-lampblack technique are carried out to qualitatively corroborate the computational flow structure with visualized patterns. Similarly the computational pressure distributions are compared with measured data.

Ashforth-Frost, S., and K. Jambunathan, (1996) Studied the Numerical prediction of semi-confined jet impingement and comparison with experimental data., San et al.,(2001),studied the "Optimum jet-to-jet spacing of heat transfer for staggered arrays of impinging air jets Aldabbagh and Sezai (2002)have investigated numerically the flow and heat transfer characteristics of impinging laminar multiple square jets showed that more uniform heat transfer can be obtained by using shower head type impinging on the surface ,Neil et al.,(2005) studied about Impingement Heat transfer : Correlations and Numerical Modeling , San, J.Y., Tsou, Y. M., and Chen, Z. C., 2007,"Studied the Impingement heat transfer of staggered arrays of air jets confined in a channel". Bernhard et al., 2009 reviewed the flow and heat transfer characteristics of multiple impinging jets and compared with single impinging jets. Rajesh Kumar panda and Prasad (2011) studied the detailed flow structure and the effect of jet-to-plate spacing for round jets on the pressure distribution and flow structure. Malladi

R.Ch. Sastry, et al., (2011), studied the fluid flow on a flat plate with three rectangular impinging slots jets

2. Experimental Details

The schematic layout of the experimental set up is shown in Fig.1. Air is supplied by a reciprocating air compressor through a calibrated Rotameter. Flow regulating and bypass valves are placed in supply line to control the flow rate. Air enters into the plenum chamber through diverging section to reduce the pressure fluctuations in air.

A seamless rectangular chamber of 600 mm length, 300 mm width and 6 mm thickness, is used as plenum chamber, whose size is large enough to is 32mm. Air ejects as jet through the orifice and impinges on the target surface. The impingement plate is of 160x160 mm in dimension. Chamber is a semi-confining plate, which contains five circular orifices of dimensions 8 mm. Air ejects as jet through the orifices and impinges on the target surface. Around the centre jet, the four perimeter jets are placed 90° apart from each other. Distance between the centre jet and perimeter jets stabilize the flow and reduce the fluctuations. Air from plenum chamber enters into the impingement air chamber which is made of 160 mm width, 160 mm height and 4mm thick mild steel square chamber. The exit side of the impingement air chamber is a semi-confining plate, which contains five circular orifices of dimensions 8 mm. Air ejects as jet through the orifices and impinges on the target surface. Around the centre jet, the four perimeter jets are placed 90° apart from each other. Distance between the centre jet and perimeter jets is 32mm. Air ejects as jet through the orifice and impinges on the target surface. The impingement plate is of 160x160 mm in dimension.

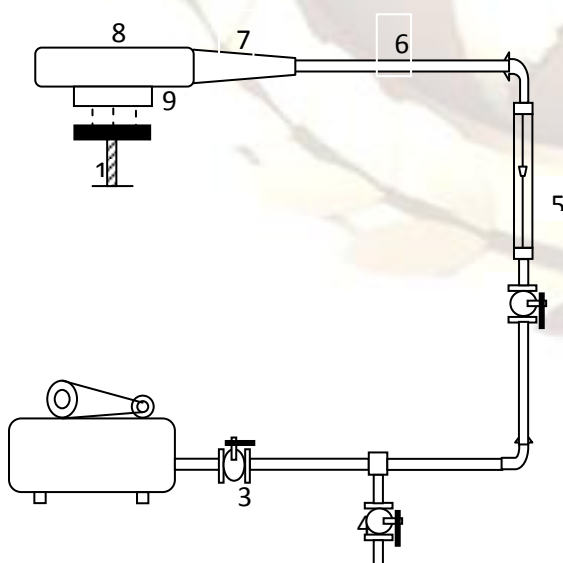
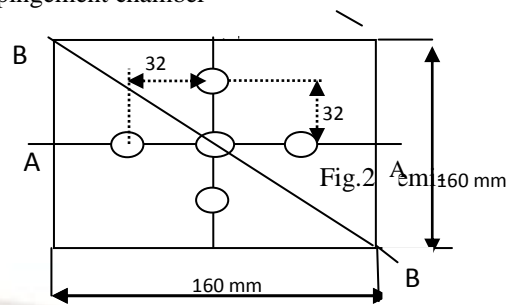


Fig. 1 Schematic diagram of experimental set-up
 (1) Test section (2) Compressor (3) Flow control valve (4) Bypass line (5) Rotameter (6) Hoss pipe

(7) Diverging section (8) Plenum chamber (9) Impingement chamber



confining plate with Dimensions

The impingement plate is of five millimeter thick acrylic sheet of 160x160 mm is used. In order to determine the non dimensional pressure distribution on the target surface, a close array of pressure tap holes of 0.8 mm diameter is drilled along the plate. The tap holes are closely placed because of the steep change of pressure expected due to jet interactions. Multi tube manometer is used for wall static pressure measurement. Impingement plate is placed over a stand, whose height can be varied by a lead screw mechanism to obtain the required h/d.

Flow visualization experiments are carried out with oil-lampblack technique. The oil and lampblack powder are mixed in proper proportion and painted on the target surface. The lampblack coated target surface is kept beneath the plenum cylinder. The air jets, after impinging on the target surface, leave traces of the flow path lines on the plate. These pictures are captured by a camera.

3. Computational Methodology

Figure 3 shows the geometric model that mimics the physical model used for experiment of Interest. It consists of a semi-confined plate and 160x160 mm square impingement plate. The semi-confining plate consists of five circular jets of 8 mm in size. The jet ejects from the circular orifice to impinge on the solid plate. Distance between the impingement plate and the jet is varied to obtain the h/d ratio from 0.5 to 4. The computational mesh suitable for finite volume method is generated by automatic grid generating tool GAMBIT 2.3.16. Non-uniform grids with clustered nodes are generated in the regions where steep gradient of velocity is expected. Optimum grid size is selected after the grid independence study.

For the purpose of computation, a specified velocity inlet condition is imposed at the entry to the orifice. A free stream turbulence intensity of 10% is chosen at the exit of orifice. The jet after hitting the plate, exits into the atmosphere in the transverse direction all around the plate periphery, where constant (ambient) pressure outlet condition is imposed. A constant heat flux value is specified at

the bottom surface of the target plate and periphery is circumferentially insulated. All the input values are those in experiment.

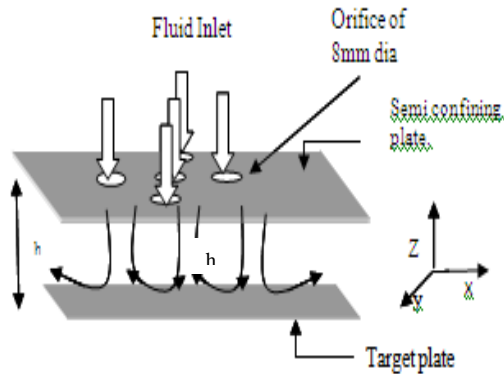


Fig. 3 Schematic Diagram of the Geometry and Boundary Conditions

The three dimensional flow is formulated with the following assumptions: (i) the fluid is incompressible, (ii) the fluid properties are constant and (iii) the mean flow is steady. The governing equations used for simulations are the Reynolds averaged continuity and momentum equations for modeling the turbulence quantities. A finite volume based solver Fluent 6.3 is used for solving the governing continuity, momentum and turbulence-model equations. SIMPLE algorithm is used for pressure velocity coupling. The solution is considered to be converged when the residual is in the order of 10^{-4} for continuity, momentum, turbulence equations and 10^{-8} for energy equations. The $\kappa-\omega$ SST model is adopted for simulation. Further area weighted average temperature of the impingement surface is continuously monitored, so that the variation will be within 1% for 1000 consecutive iterations

Continuity equation

$$\nabla \cdot (\rho \mathbf{u}) = 0$$

Momentum equation

$$(\mu \cdot \nabla) \mathbf{u} - \frac{1}{\rho} \nabla p + \nu \nabla^2 \mathbf{u} = 0$$

Turbulent kinetic energy (K) equation

$$\frac{\partial (\rho k \mu_i)}{\partial x_i} = \frac{\partial}{\partial x_j} (\Gamma_k \frac{\partial k}{\partial x_i}) + G_k - Y_k + S_k$$

Specific dissipation rate (ω) equation $\frac{\partial}{\partial x} (\rho \omega)$

$$u_i = \frac{\partial}{\partial x_j} (\Gamma_\omega \frac{\partial \omega}{\partial x_j}) + G_\omega - Y_\omega + D_\omega + S_\omega$$

Where

$$\Gamma_k = \mu + \frac{\mu_t}{\sigma_k}, \quad \Gamma_\omega = \mu + \frac{\mu_t}{\sigma_\omega}$$

μ_t

Orifice of 8mm dia

$$\sigma_{k,1} = 1.176,$$

$$\sigma_{\omega,1} = 0, \sigma_{\omega,2} = 1.168$$

Boun plate.

ed for the present study are,

i) No slip boundary condition $V_w = 0$, at $z = 0$

ii) Flow inlet condition, $V_x, V_y = 0, V_z = V_{oe}$

iii) Entrance condition, $P = P_{atm}$

The parameters investigated in the present study include (i) effect of h/d varied as 0.5, 1, 2 and 4 (ii) effect of jet exit Reynolds number, varied as 9075, 10594, 12100

3.1. Mesh

Mesh plate. is carried out to ascertain the accuracy of the numerical results. The mesh sensitivity study is carried out by analyzing the variation of static pressure distribution on the target plate along line A-A as shown in fig: it shows the pressure distribution along A-A for different mesh sizes. It is clear from the table that difference in the value of pressure with 1.58million and 1.74 million is not significant. To get advantage of computational time, mesh 1.58 million is used for this case. Similar mesh sensitivity study is done for all other cases.

Table-1

Mesh Size in Million cells	Static Pressure (Pa)
6.9	130
1.52	400
1.589	430
1.745	431

4. Results and Discussion

4.1. Flow Structure of Impinging Jet

As each of fluid jet eject out of the orifice with parabolic velocity profile a continuous reduction in velocity taken place from its center to the outer boundary. It is known that with increasing distance from exit and increasing momentum exchange between the jet and the ambient, the free boundary of jet broadens while the potential core contacts on the impingement surface, the wall jets are formed and spread radially. The wall jets emanating from each impinged form a collision front due to interaction with neighbors. Consequently an up wash flow taken place. Thus overall structure consists of (1) potential core (2) shear layer (3) wall jets (4) up wash flow etc. Figure 4 shows the velocity contours for the four jet-to-plate spacing to Jet diameter ratio namely $h/d = 0.5, 1, 2, 4$ for Reynolds number 9075.

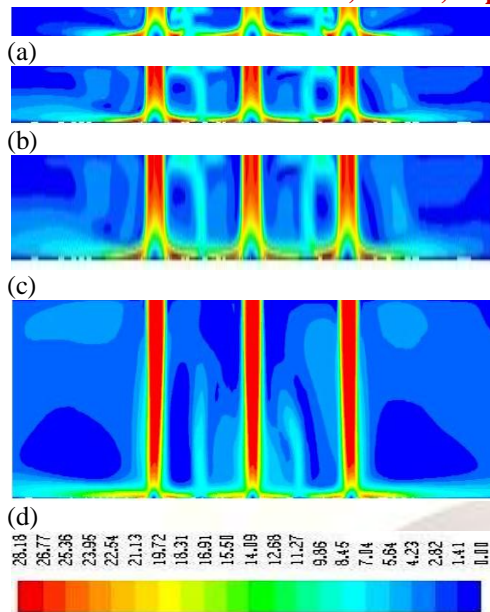


Fig. 4 Computed Velocity contours along plane A-A, for Re = 9075

(a) $h/d=0.5$, (b) $h/d=1$, (c) $h/d=2$, (d) $h/d=4$

It can be clearly seen that in case of $h/d = 0.5$ & 1 the potential core is extended up to target surface shown in Fig.4 (a & b). Whereas in case of $h/d = 2$ & 4 the potential core region vanishes by the time flow reaches the target surface, shown in Fig.4(c & d). These differences in velocity pattern happen because of the variation in momentum exchange between the fluid jet and ambient. The wall jets from adjacent jets when interacts with each other a upwash flow takes place as shown in Fig.4 when h/d value lower ($h/d = 0.5$ & 1) the interaction prominent, besides as the distance is less the upwash flow fountain reaches the top wall.

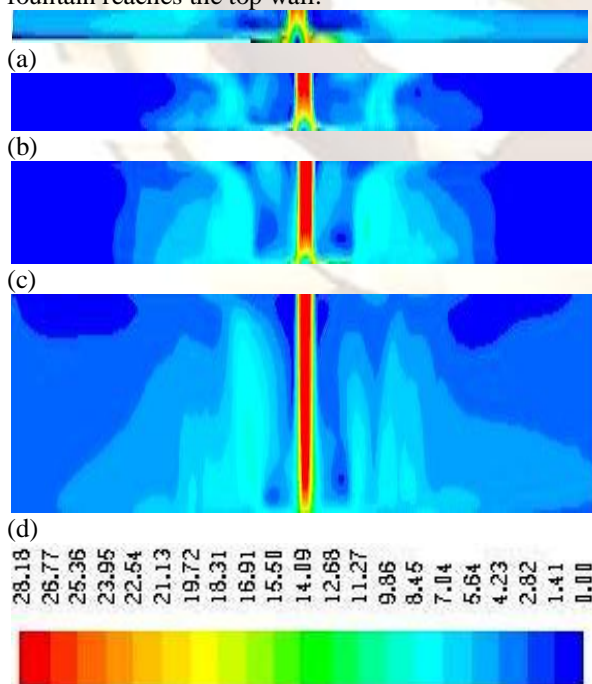
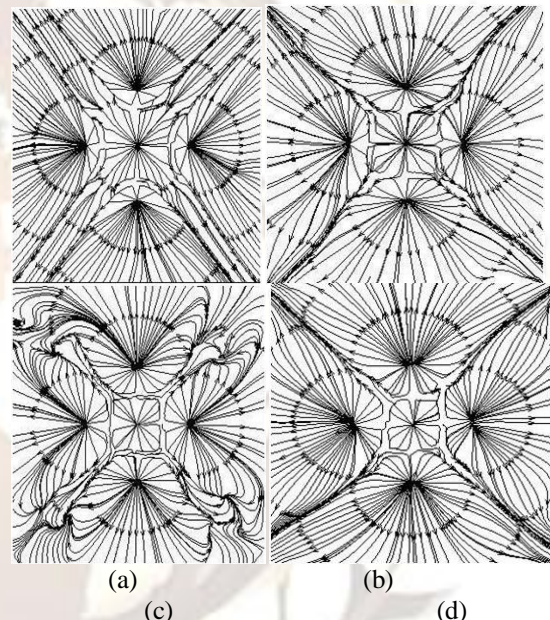


Fig. 5 Computed Velocity contours along B-B plane, for Re = 9075

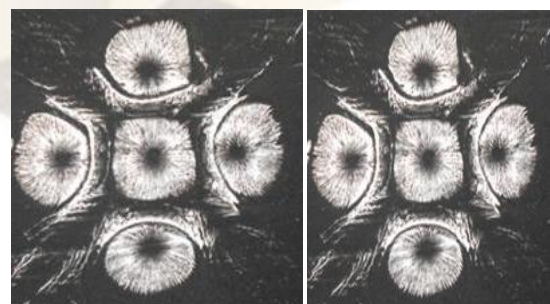
(a) $h/d=0.5$, (b) $h/d=1$, (c) $h/d=2$, (d) $h/d=4$

This low velocity jet forms another wall jets on the semi confining plate, shown in Fig. 4 (a & b). But no such thing happens for higher h/d , because the second jet diffuses out by the time it reaches the top surface, shown in Fig.4 (c & d). Fig.5 shows velocity contours along the plane B-B. The wall jets, thus separated from each other in the impingement plane by the dividing stagnation line, are shown in Figs.6 and 7, by computational surface flow lines for four h/d values of 0.5, 1, 2 and 4. The computed and experimentally visualized flow structures qualitatively agree well and hence confirm the correctness of the computation. Figure 9 shows the three dimensional separated flow. It is observed that flow separation occurs corresponding to the separation line. Mild asymmetry is observed however numerical values are perfectly symmetrical. It is observed that the position of the attachment line shifts close to the central jet as the h/d increase.



(a) $h/d=0.5$, (b) $h/d=1$, (c) $h/d=2$, (d) $h/d=4$

Fig. 6 Computed flow structure visualized as traces on impinging plate, for Re 9075



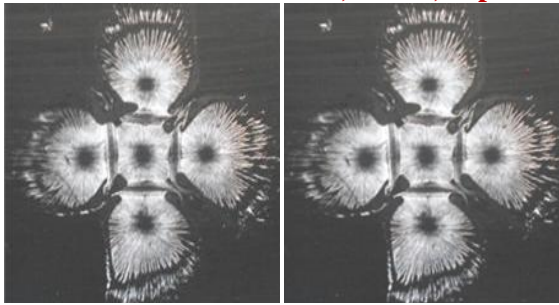


Fig. 7 Flow structure visualized as traces of oil lamp black on impingement plate, for Re 9075

(a) $h/d=0.5$ (b) $h/d=1$ (c) $h/d=2$ (d) $h/d=4$
 This may be because the flow in case of low h/d (0.5 & 1) has more momentum compare to higher h/d , hence the centre jet easily moves the surrounding fluid

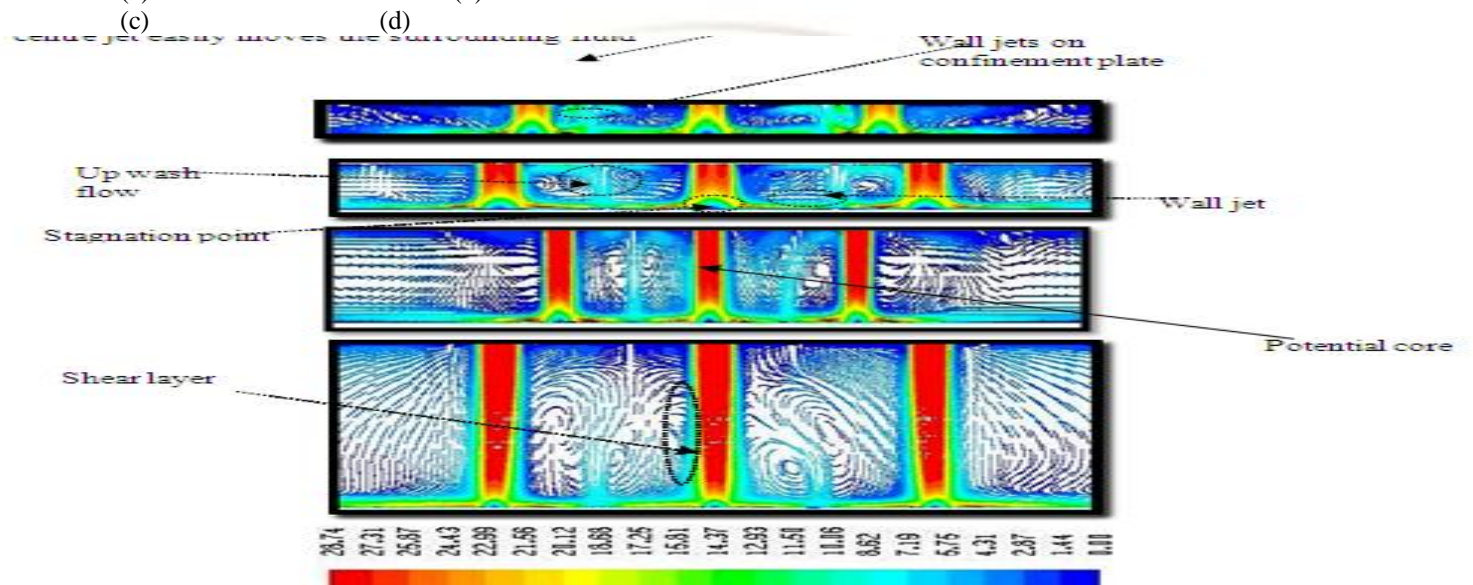


Fig 8 Path lines colored by velocity magnitude for Re = 9075 on plane A-A
 (a) $h/d=0.5$, (b) $h/d=1$, (c) $h/d=2$, (d) $h/d=4$

4.2. Comparison of Experimental and Computational Static Pressure Distribution

Figure 9 shows the comparison of non dimensional pressure distribution, between

experimental and computation along A-A the pressure distribution is observed on the impingement surface both from experiment and computation agreed with each other with in 3 %

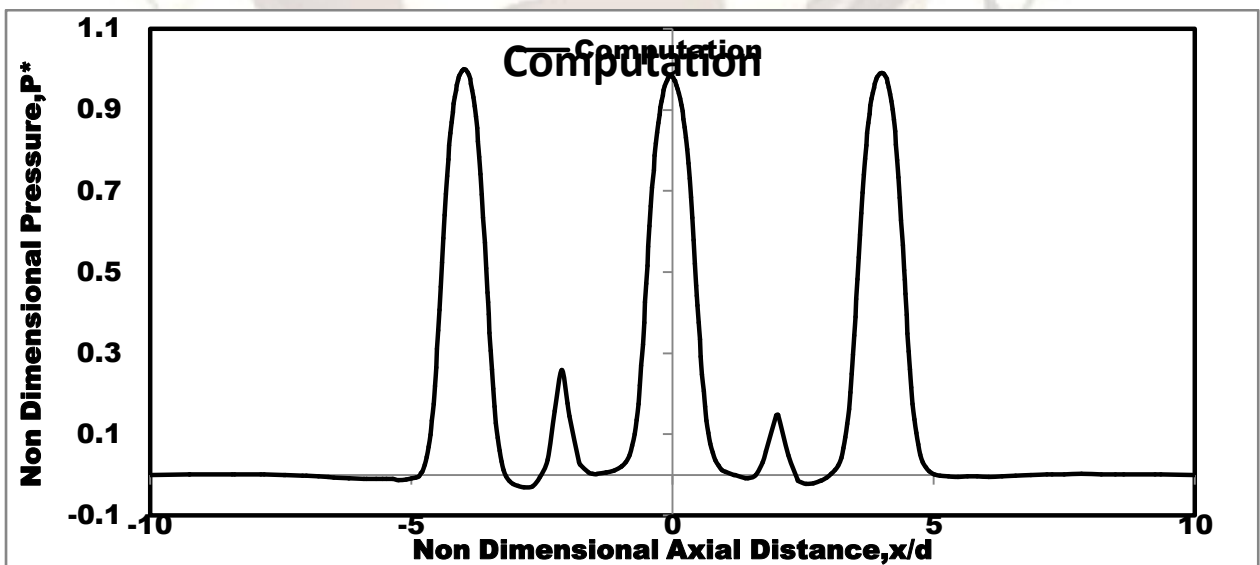


Fig. 9 Comparison non dimensional pressure

Experimental with Computation

4.3. Effect of Plate Spacing to Jet Diameter Ratio

Figure 10 shows the variation of non dimensional pressure distribution with different plates spacing to jet diameter ratio (h/d) for $Re = 9075$ in line A – A peak pressure is observed at the point of stagnation of each jet. Up wash fountain for

lower h/d is more prominent hence larger peaks are observed for lower h/d value of unity. The position of secondary peak depends upon the position of interaction point of wall jet and the size of the central square. Secondary peak moves closer to center jet with increase in h/d .

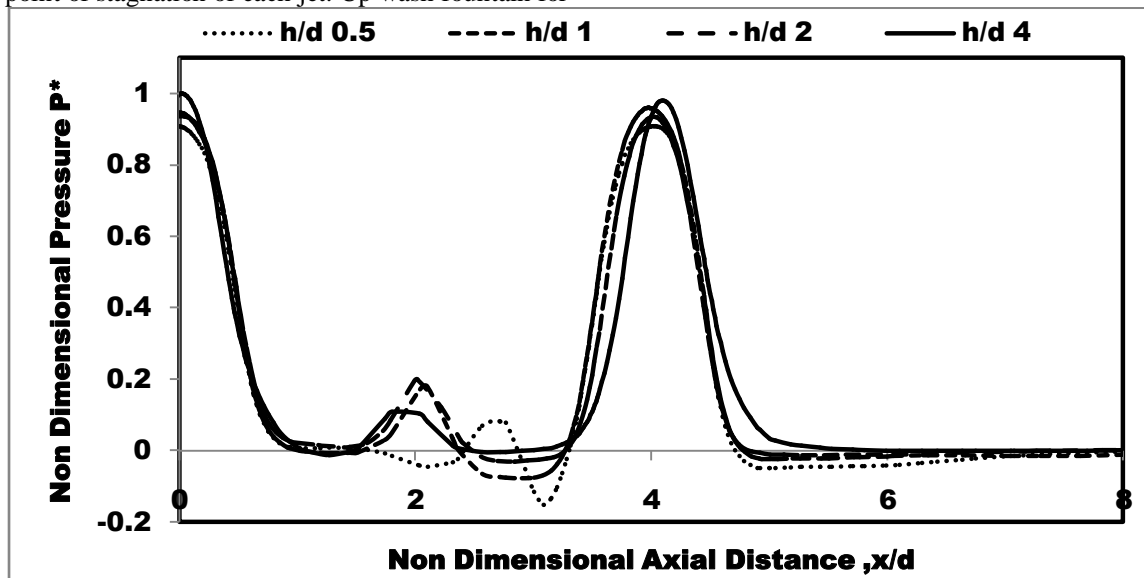


Fig. 10 Non-dimensional Pressure distribution on line A-A for varying $\frac{h}{d}$ and for $Re = 9075$

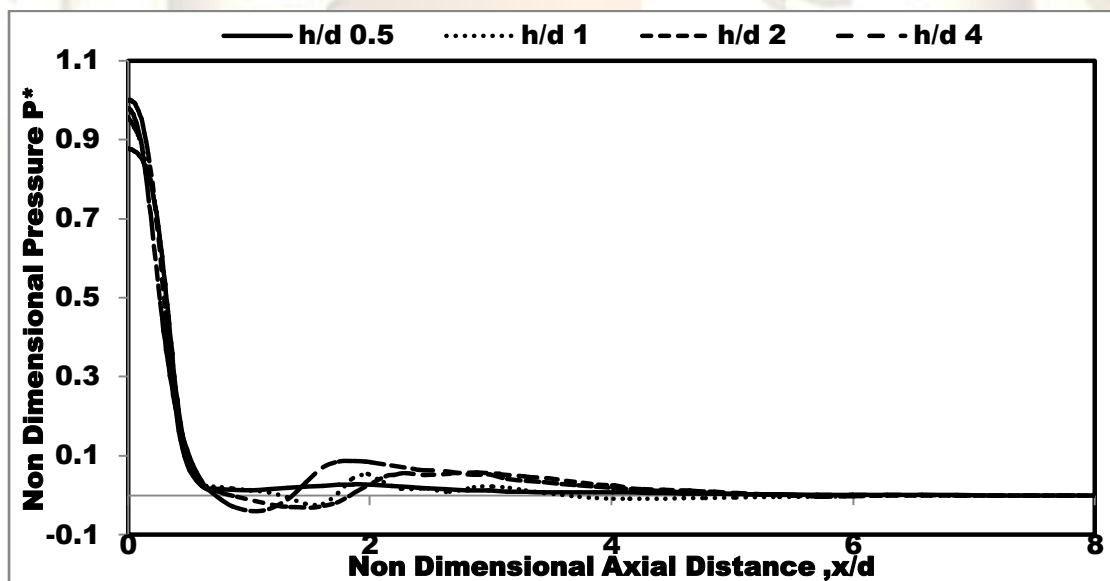


Fig. 11 Non-dimensional Pressure distribution on line B-B for varying $\frac{h}{d}$ and for $Re = 9075$

Figure 11 shows the variation of non dimensional pressure distribution in line B-B with different h/d . Here the behavior of pressure distribution in the stagnation zone is similar to the one observed in line A-A. However, unlike line A-A, up wash fountain are prominent for high h/d hence the secondary peaks are observed are large for high h/d .

4.4. Variation of Nusselt Number with Non-dimensional axial distance

The effect of plate spacing to jet diameter ratio (h/d) for $Re=9075$ and $q = 3000 \text{ w/m}^2$ in plane A-A as shown in figure. It shows that when h/d increases the Nusselt number at the stagnation region reduces for $h/d=2$ the maximum Nusselt number value in the stagnation region is lower compared to lower ($h/d=1$) by absolutely 6-7%. The difference among mussel number at the center jet is

less compared to the perimeter jet, because the perimeter jets are more affected by low temperature quiescent ambient air. If h/d is further increased the

shear layer produced by jet nozzle exists converges towards the stagnation zone and hence the Nusselt number increases at the stagnation point.

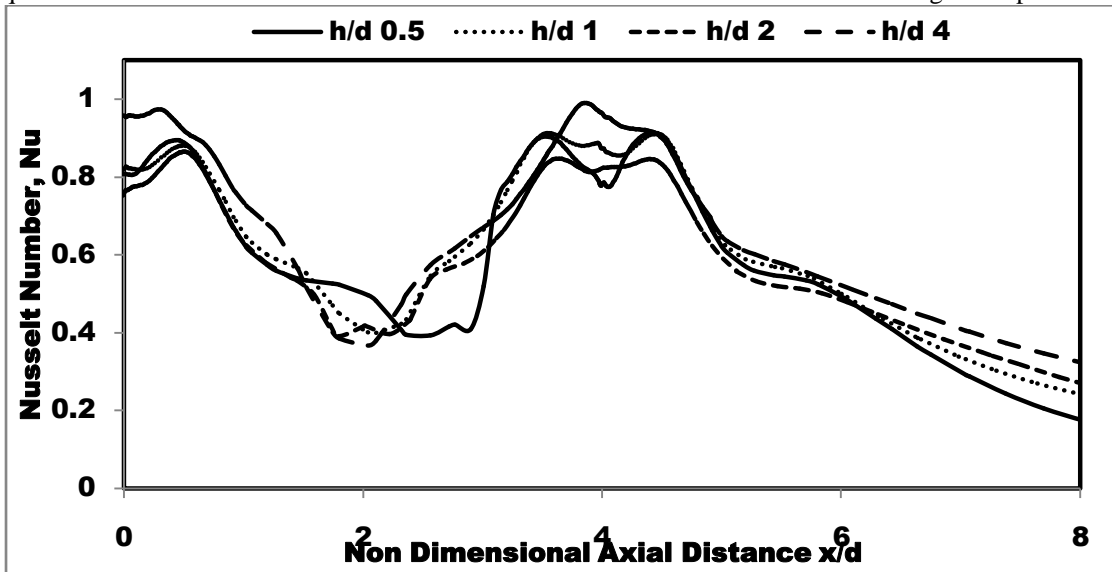


Fig. 12 Nusselt Number distribution on line A-A; for varying $\frac{h}{d}$, $q=3000 \text{ w/m}^2 \text{ k}$ and $Re=9075$

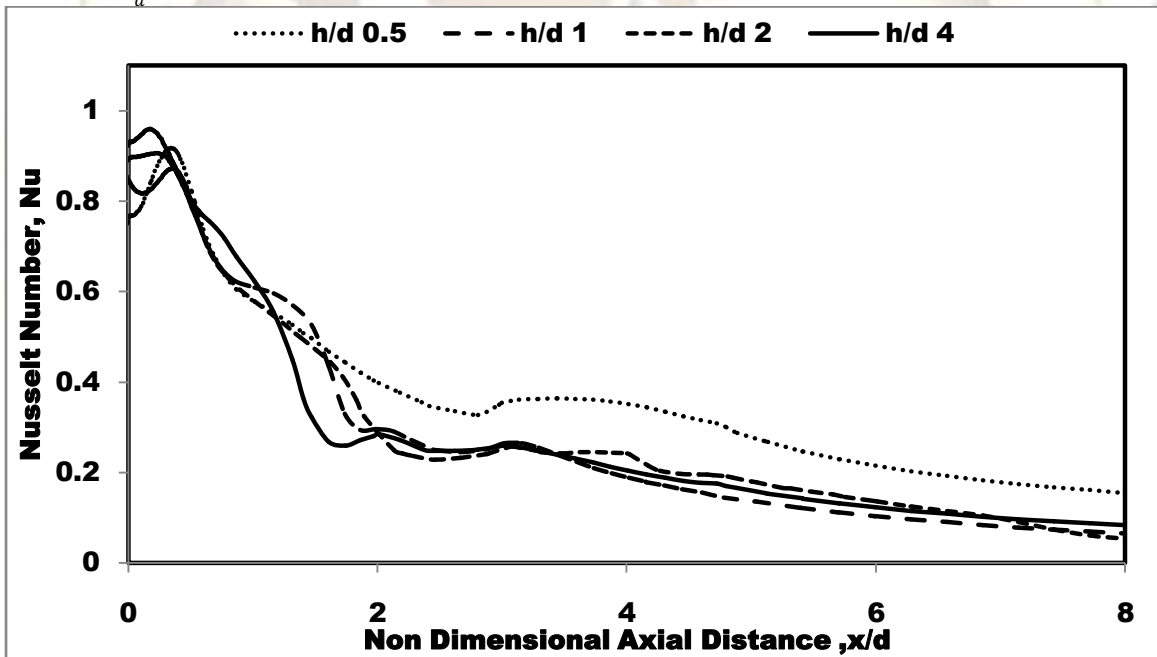


Fig. 13 Nusselt Number distribution on line B-B; for varying $\frac{H}{d}$ for $Re=9075, q=3000 \text{ w/m}^2$.

4.4. Effect of Reynolds number

Figure 14 illustrates the dependence of non dimensional pressure distribution on Reynolds number for $h/d = 2$ on line A-A. As expected the

pressure peak for higher for high Reynolds number. At any Reynolds numbers the non dimensional pressure has the high value at the stagnation region and reduces radially. Second peak is observed at the second stagnation point where neighboring wall jets collide. Position of second peak is independent of Reynolds number.

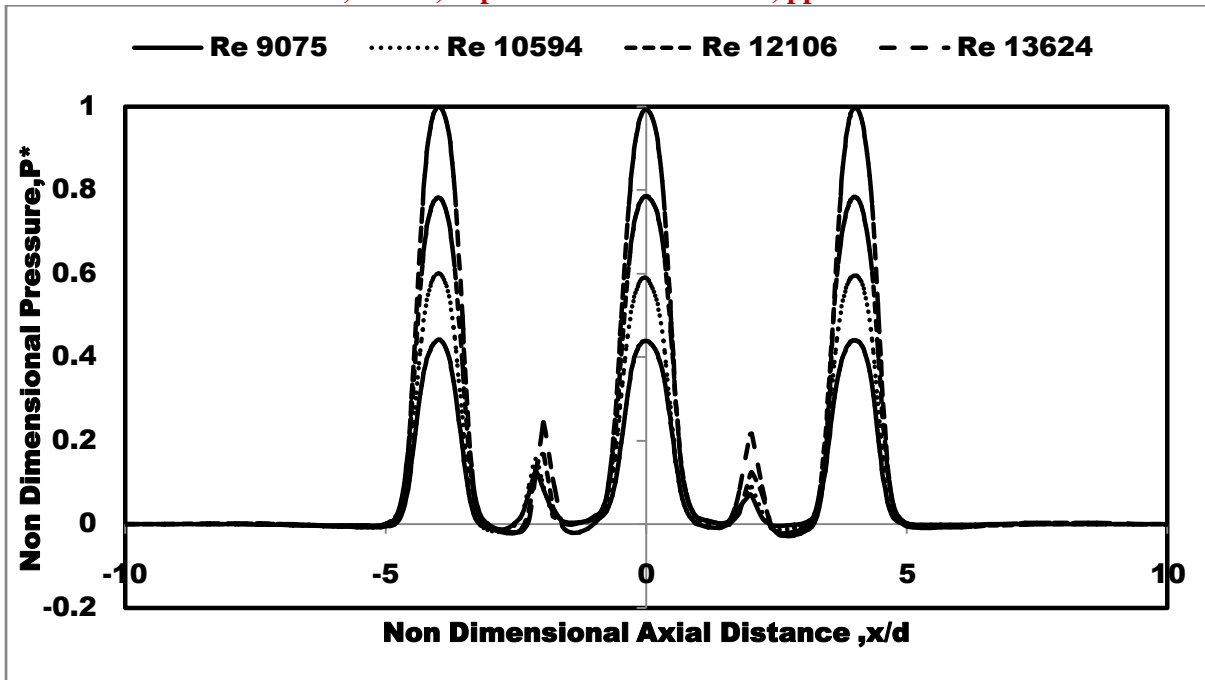


Fig. 14 Effect of Reynolds number on non dimensional pressure distribution on line A-A for $h/d=2$

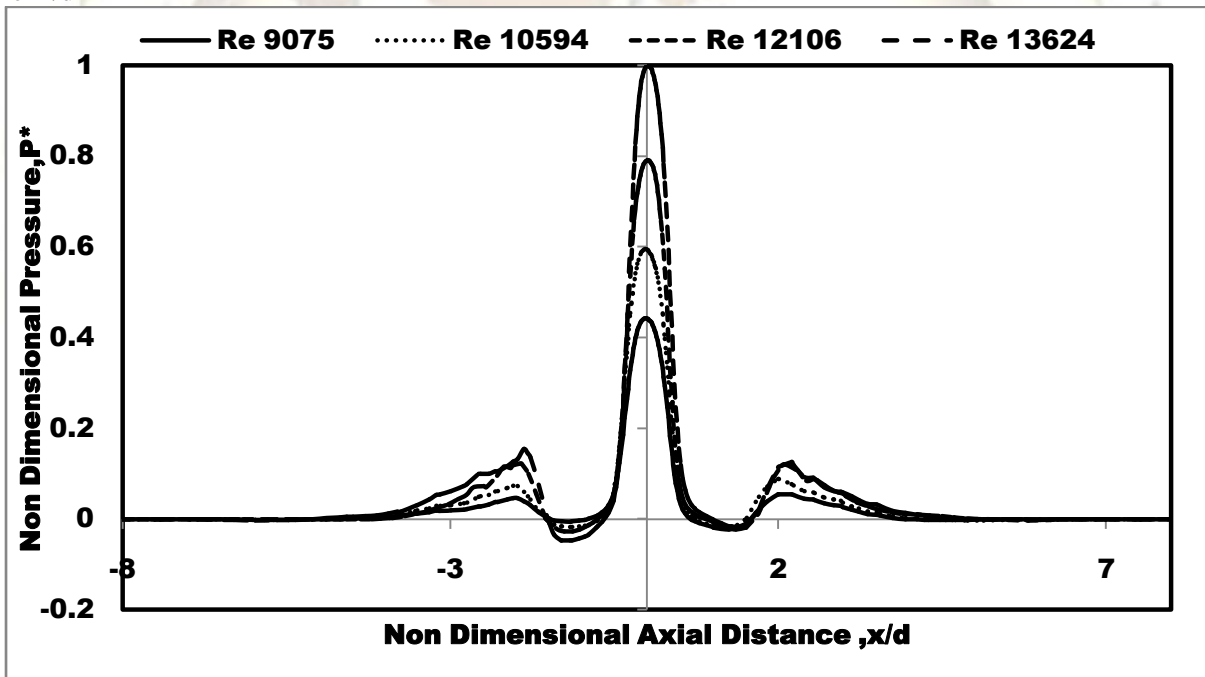


Fig. 15 Effect of Reynolds number on non dimensional pressure distribution on line B-B for $h/d=2$

Figure 15 shows the variation of non dimensional pressure distribution with different Reynolds number on line B-B. The secondary peak is formed by the interaction of wall jets is higher for high Reynolds number.

4.5. Effect of Re on Nusselt number:

Figure 16 illustrate the dependence of Nusselt number on Reynolds number for $h/d=2$ and $q=3000 \text{ w/m}^2$ on line A-A. As expected at any location heat transfer rate is higher for high Reynolds number. As the flow is independent of Reynolds number, in the range of 9075-13624. The quantitative behavior of Nusselt number. clearly indication that these trends are independent of Reynolds number .especially the position of secondary peak is Nusselt number is found at the same radial location.

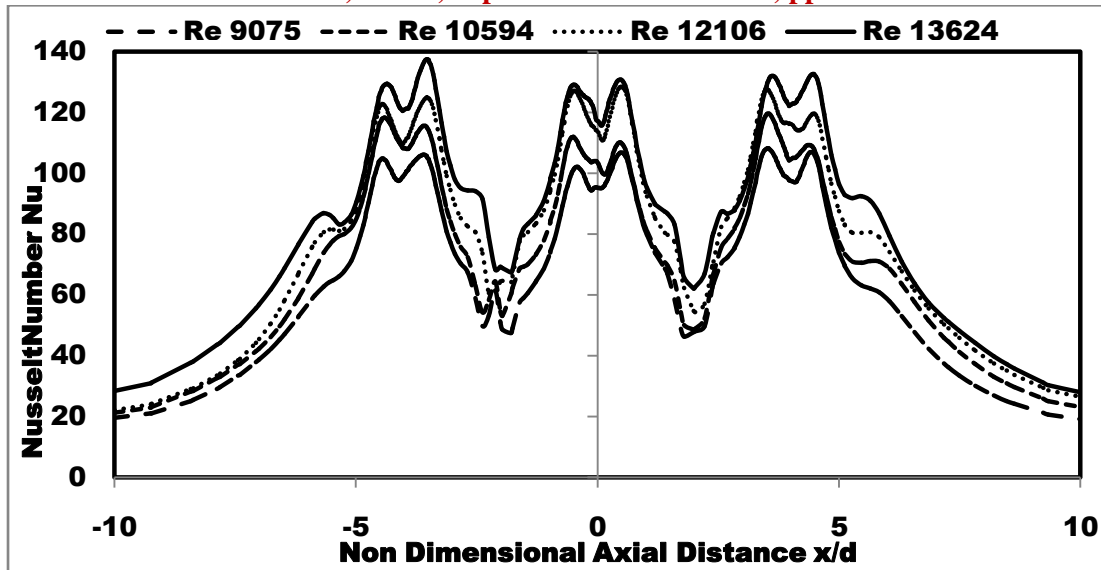


Fig. 16 Nusselt Number distribution on line A-A for varying Re for $\frac{h}{d}=2$, $q=3000\text{w/m}^2\text{k}$

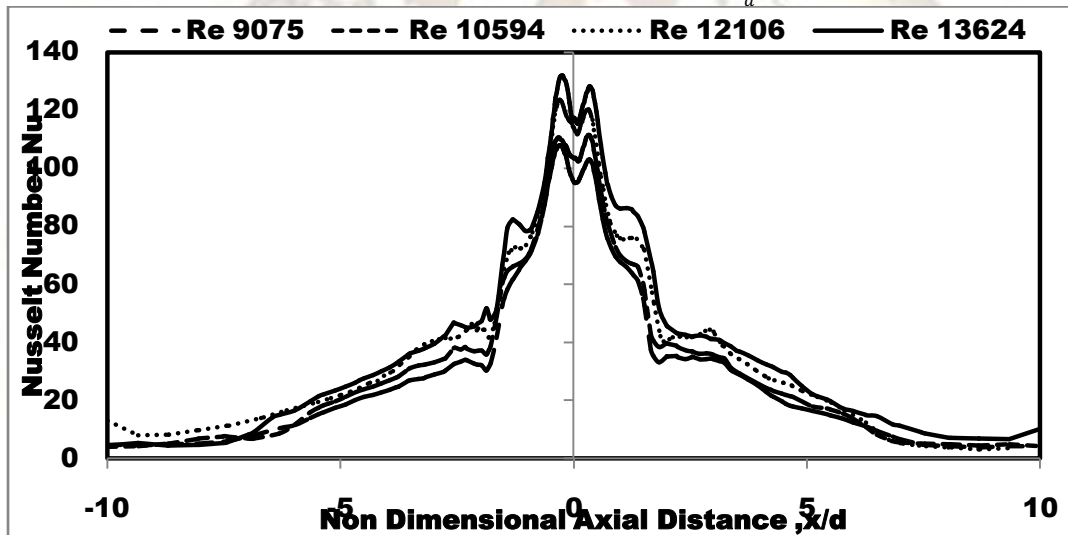


Fig. 17 Nusselt Number distribution on line B-B; for varying Re for $\frac{h}{d}=2$, $q=3000\text{w/m}^2\text{k}$

Conclusion

1. The feature of the complex flow structure are study using both oil lamp black technique and computation .computational obtained topology of flow pattern on impingement surface agree well with the experiment. It is observed that the flow topology is independent of the variation of Reynolds number in the range 9075-13624, but it altered with variation of h/d .
2. The non dimensional pressure distribution obtained from experiment is similar to computation .This validates the usage of shear stress transport (SST) (K- ω) turbulence model for the chosen problem.

3. The Nusselt on the surface is found to vary in accordance with the flow structure. Peaks are noticed in primary and secondary stagnation region. Heat transfer is low at flow separation point. It is observed that local heat transfer rate is higher for lower h/d .

4. Heat transfer rate increases with Reynolds number and position of secondary peak found to be independent of Reynolds number.

5. The heat transfer variations are clearly cor-
relatable not only with flow topology but also with dimensionless pressure distribution.

Nomenclature

d	Diameter of Jet, m
h	Jet-to-plate distance, m
P	Static Pressure, Pa
Nu	Nusselt number, Nu
P*	Non dimensional pressure
Re	Reynolds number, $\rho v d / \mu$
V _{oe}	Orifice exit jet velocity, m/s
V _z	Vertical velocity, m/s

Greek Symbols

κ	Turbulent kinetic energy, m^2/s^2
μ	Dynamic viscosity, $kg/m-s$
ρ	Density, kg/m^3
ω	Specificdissipationrate, $1/sec$
ν	Kinematicviscosity, m^2/s

Subscript

f	Fluid
o	Orifice exit
w	Wall

Abbreviations

SST	Shear Stress Transport
-----	------------------------

References

- [1] **Ashforth-Frost, S., and K. Jambunathan,** (1996) Numerical prediction of semi-confined jet impingement and comparison with experimental data, *International Journal for Numerical methods in fluids*, Vol.23, 295-306
- [2] **San, J.Y.,and M.D.Lai,**2001, "Optimum jet -to-jet spacing of heat transfer for staggered arrays of impinging air jets ",*International Journal of Heat and Mass Transfer*,44(21),pp.3997-4007.
- [3] **Aldabbagh, L.B.Y., and Sezai, I.,** 2002, "Numerical simulation of three-dimensional laminar multiple impinging square jets", *International Journal of Heat and Fluid Flow*, Vol.23, pp.509-518.
- [4] **Neil, Z., and Noam L.,** 2005, "Impingement Heat Transfer: Correlations and Numerical Modeling",*ASME Journal of Heat Transfer* ,Vol. 127,pp. 544-553.
- [5] **San, J.Y., Tsou, Y. M., and Chen, Z. C.,** 2007,"Impingement heat transfer of staggered arrays of air jets confined in a channel", *International Journal of Heat and Mass Transfer*, Volume 50, PP.3718-3727.
- [6] **Bernhard, W., and Sebastian S.,** 2009, "Multiple Jet impingement -A Review", *Int. Symp. On Heat Transfer in Gas Turbine Systems*, Turkey
- [7] **Rajesh Kumar panda and B.V.S.S.S.Prasad.,**2011 "Flow visualization and conjugate heat transfer study from Shower head impinging jets " *Proceeding of ASME-Turbo Expo 2011* ,Canada.
- [8] **Malladi R.Ch. Sastry, and A.V.S.S.K.S Gupta., B.V.S.S.S.Prasad.,** 2011,"Study of fluid flow on a flat plate with three rectangular impinging slots jets " *Proceedings of the 38th National Conference on Fluid Mechanics and Fluid Power 2011* ", MANIT, Bhopal.